THE JOURNAL OF PHYSICAL CHEMISTRY B

Article

pubs.acs.org/JPCB

Combined Application of High-Field Diffusion NMR and Molecular Dynamics Simulations To Study Dynamics in a Mixture of Carbon Dioxide and an Imidazolium-Based Ionic Liquid

Eric D. Hazelbaker,[†] Samir Budhathoki,[‡] Aakanksha Katihar,[†] Jindal K. Shah,[‡,§] Edward J. Maginn,*[,‡] and Sergey Vasenkov*[,†]

[†]Department of Chemical Engineering, University of Florida, Gainesville, Florida 32611, United States

[‡]Department of Chemical and Biomolecular Engineering, University of Notre Dame, Notre Dame, Indiana 46556, United States

[§]The Center for Research Computing, University of Notre Dame, Notre Dame, Indiana 46556, United States

Supporting Information

ABSTRACT: Self-diffusion and related short-time dynamic and structural properties were investigated for mixtures of carbon dioxide and the ionic liquid 1-*n*-butyl-3-methylimidazolium bis(trifluoromethanesulfonyl)imide [bmim]$^+$[Tf2N]$^-$ for a broad range of carbon dioxide molar fractions and at different temperatures. The studies were performed by a novel multinuclear pulsed field gradient (PFG) NMR technique, which combines the advantages of a high magnetic field (17.6 T) and a high magnetic field gradient (up to 30 T/m), in combination with molecular dynamics simulations. In general, a satisfactory agreement was observed between the experimental and simulation diffusion data. Under all conditions examined, the self-diffusion coefficients of carbon dioxide were found to be approximately an order of magnitude larger than the corresponding self-diffusion coefficients of the ions. It was observed that an increase in temperature and in the amount of carbon dioxide in the ionic liquid led to an increase in the ion self-diffusivities without changing the relationship between the self-diffusion coefficients of the cations and anions. An observation of a slightly higher diffusivity of the cations in comparison to that of the anions is attributed to the preferential mobility of the cations in the direction of the ring plane. The diffusion activation energies of the ions were found to decrease gradually with an increase of the carbon dioxide content in the ionic liquid. The activation energy of the carbon dioxide diffusion in all cases was found to be smaller than those of the ions.

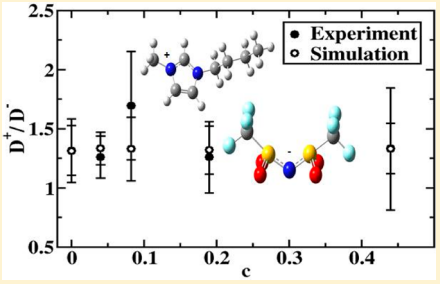

INTRODUCTION

Room temperature ionic liquids are molten salts, which are liquid at temperatures around room temperature. They exhibit a number of advantageous properties including negligible vapor pressure, high thermal and chemical stability, and high ionic conductivity.[1] The combination of these properties has made ionic liquids (ILs) a promising media for electrochemistry,[2,3] heat transfer/storage,[4] chemical reactions,[5−7] and molecular separations or storage.[8,9]

A large number of ILs exhibit high absorption capacities for light gases, including carbon dioxide. In particular, solubility of carbon dioxide in 1-*n*-butyl-3-methylimidazolium bis(trifluoromethanesulfonyl)imide [bmim]$^+$[Tf2N]$^-$ was found to be quite high.[10,11]

For applications of ILs in separations and/or storage of carbon dioxide, in addition to CO_2 sorption properties, also transport properties of the mixtures of CO_2 and ILs are of high relevance. Here we report the results of an investigation of self-diffusion in mixtures of CO_2 and [bmim]$^+$[Tf2N]$^-$ for a broad range of temperatures and carbon dioxide content by pulsed field gradient (PFG) NMR and molecular dynamics (MD) simulations. In addition, MD simulations were used to investigate a number of related dynamic and structural properties of the mixtures of CO_2 and [bmim]$^+$[Tf2N]$^-$ in order to gain a deeper insight into the transport behavior of this system. Combined application of PFG NMR and MD simulations has proven to be a useful approach for studies of dynamics in ILs.[12]

The experimental studies of self-diffusion were performed by ^{13}C PFG NMR under conditions of high magnetic field (17.6 T) and high magnetic field gradients (up to 30 T/m). Application of high gradients was essential for measurements of relatively small ion diffusivities, while high field was required for detecting sufficiently strong signal of ions by natural abundance ^{13}C PFG NMR. As a result, it was possible to measure diffusivities of ions and of ^{13}C-labeled CO_2 molecules in [bmim]$^+$[Tf2N]$^-$ in a single experiment using ^{13}C PFG NMR. Complementary ^{1}H PFG NMR studies of the cation diffusion were also carried out. ^{1}H and ^{19}F PFG NMR was previously used to study ion diffusion in a number of ionic liquids, including pure [bmim]$^+$[Tf2N]$^-$,[13] and the results presented in this paper agree with the previously reported results within the

Received: May 9, 2012
Revised: July 6, 2012
Published: July 6, 2012

   dx.doi.org/10.1021/jp304528d | *J. Phys. Chem. B* 2012, 116, 9141−9151

experimental uncertainty. ^{1}H PFG NMR was also employed to study diffusion in mixtures of ILs and small molecules such as water.[14] However, to our knowledge, no detailed PFG NMR studies of diffusion in mixtures of ILs and light gases were reported until now. Moreover, it appears that until now no data on self-diffusion in mixtures of CO_2 and ILs were measured by any technique. The majority of published experimental data on CO_2 diffusion in ILs was obtained by macroscopic techniques, which are based on measurements of gas fluxes through macroscopic IL samples. In particular, the transient thin liquid film gas uptake technique has been used to measure the transport diffusivities of carbon dioxide in several types of ILs under infinite dilution conditions. Hou et al. showed that the measured transport diffusivity of carbon dioxide in $[bmim]^+[Tf2N]^-$ was around 8×10^{-10} m^2 s^{-1} at 298 K, when averaging the results from two different $[bmim]^+[Tf2N]^-$ samples.[15] In contrast, around an order of magnitude larger values of transport diffusivity of carbon dioxide were measured by Kortenbruck et al. using FTIR in a closely related IL.[16]

MATERIALS AND METHODS

Samples. The ionic liquid 1-*n*-butyl-3-methylimidazolium bis(trifluoromethanesulfonyl)imide $[bmim]^+[Tf2N]^-$ was chosen for diffusion studies (Figure 1).

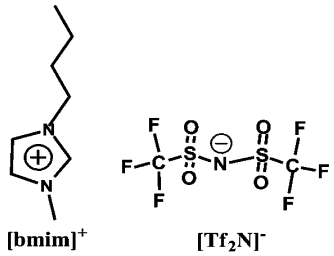

Figure 1. Atomic model of ionic liquid $[bmim]^+$ $[Tf2N]^-$.

The IL was purchased from Ionic Liquid Technologies (99% purity). The PFG NMR samples were prepared as follows. Five mm NMR tubes were filled with $[bmim]^+[Tf2N]^-$. The IL sample with the largest CO_2 loading of 0.44 CO_2 molecules per anion−cation pair, which corresponds to the CO_2 pressure in the gas phase of the sample of around 10.5 atm, was prepared in an M series 5 mm NMR tube (Southern Scientific, Inc.). For all other samples, P series 5 mm NMR tubes (Southern Scientific, Inc.) were used. In all cases the sample height in a vertically oriented tube was around 12 mm or smaller to prevent the disturbing influence of convection effects on the data measured at elevated temperatures. The IL samples were dried and loaded with CO_2 using a custom-made vacuum system. The removal of water from the IL was performed by keeping the samples at around 373 K under high vacuum for at least 1 day as discussed in our previous work.[14] The loading was carried out by freezing CO_2 from the calibrated volume of the vacuum system into the NMR tube with the sample using liquid nitrogen. The NMR tubes were flame-sealed after loading was complete. The concentration of carbon dioxide inside the IL was calculated using the following data: (i) Henry's law constants reported in ref 15. for carbon dioxide absorption into $[bmim]^+[Tf2N]^-$, (ii) known mass of CO_2 introduced into the tubes with the IL before they were sealed, and (iii) known volumes of the IL and the gas phase in the sealed NMR tubes.

Pulsed Field Gradient (PFG) NMR Studies. PFG NMR is a powerful technique for self-diffusion studies.[17,18] ^{13}C and ^{1}H PFG NMR diffusion studies were performed using a wide bore 17.6 T Bruker Biospin spectrometer. The magnetic field gradients were generated using a diff60 diffusion probe (Bruker Biospin) and a Great60 gradient amplifier (Bruker Biospin). The ^{13}C PFG NMR measurements were performed using the standard PFG NMR stimulated echo pulse sequence (PFG NMR STE),[17,18] and the ^{1}H PFG NMR experiments were done using the PFG NMR 13-interval sequence.[19] The latter sequence allows reducing or even eliminating the disturbing influence of the magnetic susceptibility effects on the measured data by using gradients of opposite polarity. Observation of coinciding diffusion data measured by these two sequences for the same species, in the same sample, and under the same measurement conditions was used to rule out any influence of the magnetic susceptibility effects and other disturbing measurement effects on the reported results.

Diffusion data were obtained from PFG NMR attenuation curves, viz., dependencies of the intensity of the PFG NMR signal (A) on the amplitude of the magnetic field gradients (g). The signal intensity corresponds to the amplitude of a selected line of a spectrum recorded by PFG NMR sequence. The measured ^{13}C spectra of the mixtures of $[bmim]^+[Tf2N]^-$ and CO_2 contain lines from all three of the diffusing species, i.e., the $[bmim]^+$ cation, the $[Tf2N]^-$ anion, and CO_2. In contrast, the proton PFG NMR spectra of such samples exhibit only the cation lines because the other two species do not contain any hydrogen atoms. Diffusion data for each type of species was obtained by choosing one or more NMR lines originating from these species for data processing. For each such line the self-diffusivity (D) was determined from the attenuation curves of the PFG NMR signal ($\psi \equiv A(g)/(A(g{=}0))$) using[17−19]

$$\Psi = \exp(-q^2 t_{\text{eff}} D) \tag{1}$$

where $q = \gamma\delta g$ for the PFG NMR STE sequence and $q = 2\gamma\delta g$ for the PFG NMR 13-interval sequence, γ is the gyromagnetic ratio, δ denotes the duration of the field gradient pulses, and t_{eff} is the effective diffusion time defined in references 17−19. In cases when several sufficiently strong NMR lines can be recorded for the same diffusing species, it was verified that the attenuation curves and the corresponding diffusivities obtained by using different lines originating from the same species are the same within the experimental uncertainty of the measurement. In each case the PFG NMR attenuation curves were measured for at least two diffusion times (8.6 and 38.6 ms) to rule out an occurrence of convection effects under our measurement conditions. The high-field diffusion NMR technique used in this study provides superior sensitivity allowing us to not only measure the ^{13}C PFG NMR attenuation curves for the ^{13}C-enriched species (carbon dioxide) but also the $[bmim]^+$ cation and $[Tf2N]^-$ anion by natural abundance ^{13}C PFG NMR.

Simulation Methods. An all-atom force field of the following functional form was used for the MD simulations

dx.doi.org/10.1021/jp304528d | J. Phys. Chem. B 2012, 116, 9141−9151

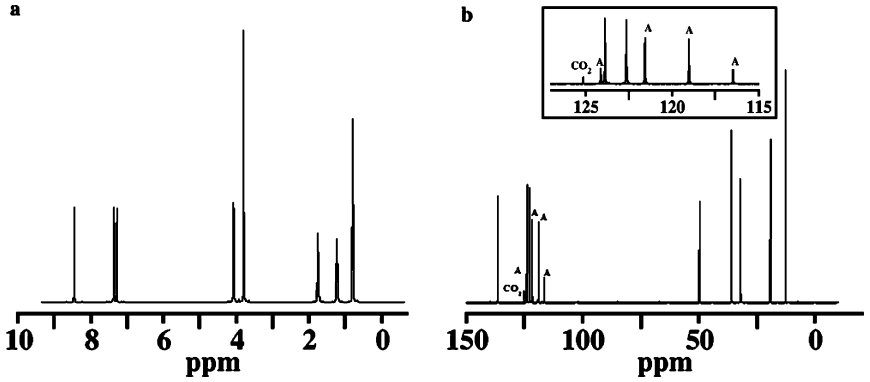

Figure 2. NMR spectra of $[bmim]^+[Tf2N]^-$ containing 0.011 carbon dioxide molecules per anion−cation pair. The spectra were recorded by ^1H NMR one-pulse sequence (a), and by ^{13}C NMR one-pulse sequence (b). The ^1H and ^{13}C chemical shifts were referenced internally to HDO, viz., D_2O in H_2O mixture. In the proton spectrum all lines originate from the $[bmim]^+$ cation. In the carbon-13 spectrum the four recorded lines of the $[Tf2N]^-$ anion are labeled by "A" and the single carbon dioxide line is labeled by "CO_2". All other lines in the ^{13}C spectrum originate from the $[bmim]^+$ cation.

$$V_{tot} = \sum_{bonds} k_b(r - r_0)^2 + \sum_{angles} k_\theta(\theta - \theta_0)^2 + \sum_{dihedrals} k_\chi[1 + \cos(n\chi - \delta_\chi)] + \sum_{improper} k_\psi[1 + \cos(n\psi - \delta_\psi)] + \sum_{i=1}^{N-1}\sum_{i<j}^{N}\left\{4\epsilon_{ij}\left[\left(\frac{\sigma_{ij}}{r_{ij}}\right)^{12} - \left(\frac{\sigma_{ij}}{r_{ij}}\right)^{6}\right] + \frac{q_i q_j}{4\pi\epsilon_0 r_{ij}}\right\} \quad (2)$$

where the terms have their usual meaning.[20]

For the IL, the force field parameters for bonds, angles, and improper terms and the Lennard-Jones parameters were obtained from the Generalized Amber Force Field (GAFF).[21] The Lorentz−Berthelot combining rule was used to generate Lennard-Jones parameters for unlike atoms. As is customary with GAFF, the intramolecular van der Waals and electrostatic interactions for atoms separated by exactly three bonds were scaled by a factor of 0.5 and 0.83. The electronic structures of the cation and anion were obtained by performing geometry optimization on an isolated cation and anion with the Gaussian 09 package[22] using B3LYP/aug-cc-pVDZ basis set. The restrained electrostatic potential method (RESP)[23] was used to obtain partial atomic charges. Based on our previous work in which it was shown that charge scaling improves the agreement between the calculated diffusivities from simulations and experimental data,[24] a uniform scaling of 0.8 was used for the cation and anion charges. Quantum mechanics (QM) and molecular mechanics (MM) methods were used to parameterize dihedral angles. In the QM method, dihedral angles were optimized using B3LYP/aug-cc-pVDZ followed by a single-point calculation using MP2/aug-cc-pVDZ. Then MM dihedral scans were performed in which the dihedral angle of interest was restrained to the value found in the QM calculation, while every other degree of freedom was allowed to relax to an energy minimum. The partial charges, bond lengths, and Lennard-Jones potential parameters for CO_2 were taken from the TraPPE[25] force field. The force constants for the bond and angle of CO_2 were taken from the work of Shi et al.,[26] thereby rendering it flexible.

MD simulations were carried out for pure IL and its mixture with CO_2 using the software LAMMPS.[27] In all the simulations, 250 anion−cation pairs of IL were used. The system was studied at three temperatures, 298, 333, and 351 K, and CO_2 to IL mole ratios (c) of 0.04, 0.08, 0.19, and 0.44. Simulation CO_2 compositions were matched with the experiment, and Henry's constant[15] was used to set the pressure for a given composition. The Henry's constant at 333 and 351 K were obtained by linear extrapolation of the experimental data.

Initial configuration was generated by inserting IL and CO_2 molecules into a periodic cubic box, and the energy of the system was minimized using a conjugate energy minimization technique. Next, a random velocity was assigned, and the system was equilibrated for 40 ps in the canonical (NVT) ensemble in order for it to reach the desired temperature. The temperature during the course of the simulation was controlled using a Nosé−Hoover thermostat with a damping factor of 0.1 ps. The NVT simulation was followed by a 7 ns simulation in the isothermal isobaric (NPT) ensemble in which the pressure was maintained using a Nosé−Hoover barostat with a damping factor of 1 ps^{-1}. The final 2 ns of this run were used to calculate the densities. For the calculation of transport properties, the average volume calculated from the NPT simulation was used in a subsequent NVT 40 ps equilibration followed by a 10 ns simulation in the microcanonical (NVE) ensemble from which trajectories were taken for analysis.

The Lennard-Jones and electrostatic interactions were truncated at 12 Å. The long-range electrostatic interactions were handled using the particle−particle particle-mesh Ewald method. A time step of 1 fs was used. Coordinates were recorded every 20 ps and the velocities every 50 fs.

RESULTS AND DISCUSSION

Self-Diffusion Properties by PFG NMR and MD Simulations. Figure 2 shows examples of the ^1H and ^{13}C NMR spectra obtained by one pulse sequence for a mixture of $[bmim]^+[Tf2N]^-$ and CO_2. In the ^1H NMR spectrum (Figure 2a), all the lines originate from the $[bmim]^+$ cation. The strongest lines in this spectrum at 8.5, 7.3, 3.8, and 0.8 ppm were used for determining the cation diffusivity by ^1H PFG NMR. The ^1H PFG NMR diffusivities reported below were averages over diffusivities obtained using the four lines. For each measurement the diffusivities corresponding to these lines were found to coincide within the experimental uncertainty.

dx.doi.org/10.1021/jp304528d | J. Phys. Chem. B 2012, 116, 9141−9151

The ^{13}C NMR spectrum (Figure 2b) contains contributions from the $[bmim]^+$ cation, the $[Tf2N]^-$ anion, and CO_2. A single CO_2 line at 125 ppm and four lines of the anion at 124.1, 121.6, 119, and 116.5 ppm are labeled in the figure. All other lines in the ^{13}C spectrum correspond to the cation. The lines used in the self-diffusivity calculations for the anion are at 121.6 and 119 ppm, and for the cation the lines used are at 136.4, 49.8, 32, and 19.3 ppm. These lines were selected because they are the strongest pure (i.e., nonoverlapping) lines of the ions (Figure 2b). In complete analogy with the ^1H PFG NMR data, the reported below ^{13}C PFG NMR diffusivities were obtained by averaging over diffusivities corresponding to these lines. Under our measurement conditions, the difference between each average value and the corresponding diffusivities resulting from the individual lines did not exceed the reported experimental uncertainty.

It was observed that in all cases the PFG NMR attenuation curves were monoexponential in agreement with eq 1. Figures 3 and 4 show examples of the measured attenuation curves. It was verified that the diffusion data do not depend on the nuclei type (^1H or ^{13}C) used for the diffusion measurements. This is demonstrated in Figure 3. This figure shows a comparison of the attenuation curves measured by ^1H PFG NMR and ^{13}C PFG NMR for the $[bmim]^+$ cation in CO_2-free $[bmim]^+[Tf2N]^-$. According to eq 1, in the presentation of this figure the coinciding curves indicate that the same diffusivities are recorded by using both nuclei. The observed agreement between the data obtained by ^1H and ^{13}C PFG NMR provides solid evidence that under our experimental conditions the diffusion data were not perturbed by the magnetic susceptibility or any other disturbing measurement effects.

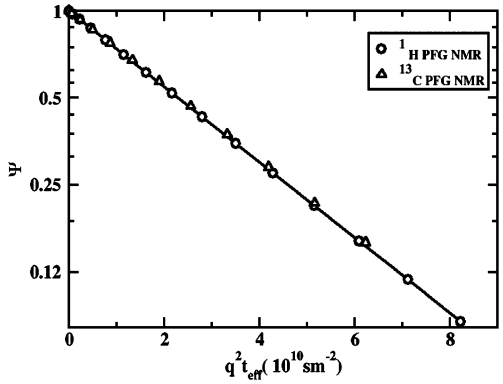

Figure 3. Examples of PFG NMR attenuation curves obtained for diffusion of the $[bmim]^+$ cation in pure $[bmim]^+[Tf2N]^-$ for t_{eff} = 8.6 ms at 297 K by the ^{13}C PFG NMR STE and ^1H PFG NMR 13-interval pulse sequences. The attenuation curves were obtained by averaging the corresponding attenuation curves measured for the cation lines at 8.5, 7.3, 3.8, and 0.8 ppm by ^1H PFG NMR and at 136.4, 49.8, 32, and 19.3 ppm by ^{13}C PFG NMR. The line shown is the best fit result using eq 1 for the ^1H PFG NMR data.

Figure 4 shows examples of ^{13}C PFG NMR attenuation curves for a mixture of $[bmim]^+[Tf2N]^-$ and ^{13}C-labeled carbon dioxide. According to eq 1 the slopes of the attenuation curves in the presentation of this figure correspond to the values of self-diffusivities. Hence, Figure 4 demonstrates that the diffusivity of the cation is larger than that of the anion, but, at the same time, much smaller than the diffusivity of CO_2. Qualitatively, the same relationships between the diffusivities of

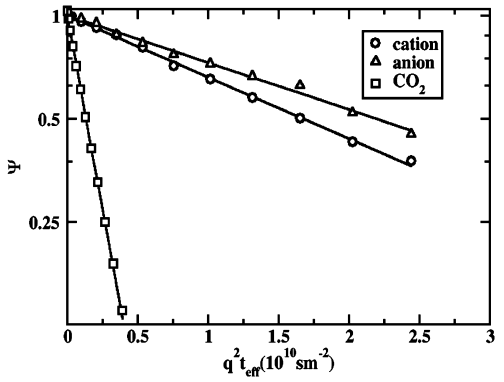

Figure 4. ^{13}C PFG NMR attenuation curves obtained by the ^{13}C PFG NMR STE sequence for the mixture of $[bmim]^+[Tf2N]^-$ with CO_2 for t_{eff} = 8.6 ms at 297 K. The attenuation curves for the ions were obtained by averaging the corresponding attenuation curves measured for the following NMR lines: lines at 136.4, 49.8, 32, and 19.3 ppm for the cation, and lines at 121.6 and 119 ppm for the anion. The attenuation curve for CO_2 corresponds to the single CO_2 line at 124.7 ppm. The number of carbon dioxide molecules per anion−cation pair in the sample is equal to 0.19. The lines show the best fit results using eq 1.

these three species were also observed at other temperatures and CO_2 loadings used in this work.

The corresponding self-diffusion data for the ions and CO_2 were also obtained using MD simulations. The self-diffusivities were calculated from the center of mass mean square displacement (MSD) of each of the species, given by

$$\mathrm{MSD} = \langle |r(t) - r(0)|^2 \rangle \tag{3}$$

where $r(t)$ is the position of a species at time t and $r(0)$ is the position at time $t = 0$. The brackets $\langle ... \rangle$ denote the ensemble average over the configurations of the system and time. The self-diffusion coefficients were calculated based on the MSD data obtained between 0.6 and 1 ns and using the Einstein relationship

$$D = \lim_{t\to\infty} \frac{1}{6t} \langle |r(t) - r(0)|^2 \rangle \tag{4}$$

Table 1 summarizes all the self-diffusion coefficients obtained by PFG NMR and MD simulations. Uncertainties of the values obtained by the simulations were computed from the standard deviation of four independent simulation runs for each case. Uncertainties of the experimental values in the table were estimated taking into account deviations between the diffusivities obtained for the same species using different NMR lines and/or different diffusion times under otherwise the same conditions. The experimental uncertainties of the diffusivities at $T > 298$ K are in most cases higher than those at $T = 298$ K because of the following reason. The PFG NMR measurements were performed with mixtures of the IL and CO_2 located inside sealed NMR tubes. As the temperature of a tube with the sample is increased there is a desorption of CO_2 from the IL into the gas phase of the tube causing the actual CO_2 concentration in the IL to be lower at $T > 298$ K than at $T = 298$ K. Such loss of CO_2 causes the diffusivities measured at $T > 298$ K to be smaller than those expected under the conditions of no concentration change. This effect was taken into account by showing larger uncertainties of the experimental diffusivities in Table 1 for $T > 298$ K. To estimate these uncertainties the temperature-induced decrease in the CO_2 concentration was

dx.doi.org/10.1021/jp304528d | J. Phys. Chem. B 2012, 116, 9141−9151

Table 1. Self-Diffusion Coefficients ($D \times 10^{10}$ m^2/s)[a] in [bmim]$^+$[Tf2N]$^-$–CO_2 Mixtures for Different Numbers of Carbon Dioxide Molecules Per Anion–Cation Pair (c) and at Different Temperatures

		simulation			experiment			% difference		
T (K)	c	CO_2	cation	anion	CO_2	cation	anion	CO_2	cation	anion
298	0	–	0.13_1	0.10_1	–	0.29_2	0.21_2	–	55.2	52.4
	0.04	1.7_2	0.13_1	0.10_1	3.7_2	0.29_1	0.23_1	54.1	55.2	56.5
	0.08	2.0_2	0.16_2	0.12_1	4.1_2	0.31_1	0.24_4	51.2	48.4	50.0
	0.19	2.4_1	0.19_2	0.15_1	5.0_2	0.39_4	0.31_2	52.0	51.2	51.6
	0.44	3.2_3	0.26_5	0.20_4	5.5_2	0.44_3	0.33_2	41.8	41.0	39.3
333	0	–	0.47_2	0.35_2	–	1.06_5	0.82_4	–	55.7	57.3
	0.04	5.4_2	0.50_1	0.38_1	8.6_7	1.04_1	0.84_3	37.2	51.9	54.8
	0.08	5.5_3	0.52_2	0.38_2	9.8_6	1.1_1	0.83_1	43.9	52.7	54.2
	0.19	6.0_3	0.62_4	0.46_2	11_2	1.1_2	0.9_2	44.5	43.6	48.8
	0.44	8.0_1	0.86_4	0.64_4	11.1_6	1.1_2	0.89_6	27.9	21.8	28.1
351	0	–	0.75_4	0.56_4	–	1.71_7	1.44_1	–	56.1	61.1
	0.04	7.7_4	0.86_4	0.64_3	11.6_3	1.53_6	1.3_2	33.8	43.8	50.8
	0.08	8_1	0.86_4	0.65_3	13_2	1.75_7	1.31_7	38.5	50.9	51.1
	0.19	8.9_7	1.0_1	0.72_7	16_3	1.9_4	1.7_4	44.4	47.4	57.6
	0.44	10.5_8	1.2_1	0.93_9	16_3	1.9_4	1.6_2	34.4	36.8	41.9

[a]Uncertainties in the last digits are indicated by subscripts in all tables.

obtained from measurements of the area under the CO_2 NMR line. In particular, it was found that in the sample with c = 0.19 at T = 298 K the CO_2 concentration in the IL becomes smaller by a factor of 2.3 when the temperature is increased from 298 to 351 K. Such concentration decrease at a fixed temperature of 298 K was observed to make the CO_2 diffusivity smaller by a factor of around 1.2.

The data in the table show that the simulated self-diffusivities are about 50% lower than the experimental values, although the simulations correctly reproduce the trend obtained in the experiments. The reduced dynamics compared to the experiments is consistent with previous simulation studies[28,29] where it was shown that neglect of polarizability and charge transfer through the use of a fixed charge model leads to reduced dynamics. Recent ab initio simulations[30,31] have shown that the net charge on ions in the liquid phase is less than unity. The use of scaled charges attempts to capture this effect, and it does enhance the mobility of the ions.[24]

It can be readily seen that the diffusion coefficient of CO_2 is almost an order of magnitude greater than those of the cation and anion. It can also be noted that the cation diffuses faster than the anion. Hence, $D_{CO_2} > D_{cation} > D_{anion}$. According to Ribeiro and Urahata,[32] who carried out an anisotropic ionic displacement study of imidazolium-based ILs, the higher diffusivity of cations is due to their preferential mobility in the direction of the ring plane, almost perpendicular to the long alkyl chain. The preferred model of diffusion in this study was shown at 400 K. Liu and Maginn[24] demonstrated, from MD simulations, that the higher mobility of the cation at temperatures below 400 K arises mainly due to the preferred mobility of [bmim]$^+$ along the direction of the alkyl chain. Figure 5 demonstrates that for the range of CO_2 concentrations studied, the ratio of the self-diffusivities for the cation and anion remains the same within the uncertainty. Moreover, the simulations and experiments are in excellent agreement for the ratio D_{cation}/D_{anion}.

It was found that the self-diffusion coefficient of each species increases with increasing amount of CO_2. Figure 6 demonstrates such a trend at 297 K. These data suggest that CO_2 fluidizes the system. This is also supported by the decrease in

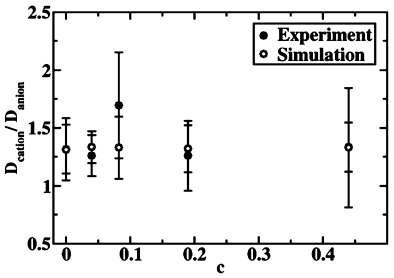

Figure 5. Dependence of the ratio of the cation self-diffusivity to the anion self-diffusivity on the number of carbon dioxide molecules per anion–cation pair (c) in the mixture of [bmim]$^+$[Tf2N]$^-$ with CO_2 at 298 K. The data were obtained by ^{13}C PFG NMR and by MD simulation.

the density of the system as will be discussed later. Using simulations,[33] it was shown that CO_2 tends to associate with [Tf2N]$^-$ more strongly than with the [bmim]$^+$ cation. Thus, it is likely that the interaction between the cations and anions is weakened by the addition of CO_2, thereby making the ions more mobile as CO_2 concentration increases.

It was observed that in the measured temperature range the temperature dependencies of the cation, anion, and carbon dioxide diffusivities in each studied sample can be described satisfactorily by the Arrhenius law

$$D = D_0 \exp\left(-\frac{E_a}{RT}\right) \quad (5)$$

where E_a is the activation energy of diffusion. Figure 7 shows examples of the temperature dependencies of the diffusivities obtained by ^{13}C PFG NMR and MD simulations.

Table 2 presents the activation energies of diffusion for the cation, anion, and carbon dioxide for different CO_2 content in [bmim]$^+$[Tf2N]$^-$. It is seen that the activation energy of CO_2 is lower than that of the cation and anion, which can be explained by the fact that CO_2 is smaller than the ions and also associates less strongly. In the case of the cation and anion, the activation energy is higher due to strong electrostatic interactions between the counterions. The activation energies of the cation and anion are nearly identical, and the agreement between simulation and

dx.doi.org/10.1021/jp304528d | J. Phys. Chem. B 2012, 116, 9141–9151

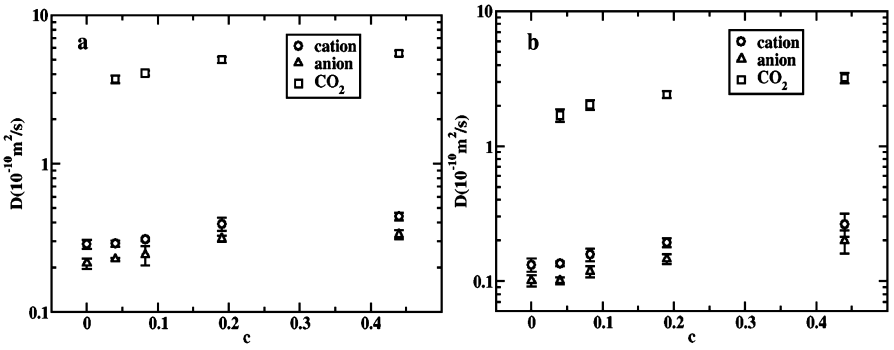

Figure 6. Self-diffusivities of the $[bmim]^+$ cation, the $[Tf2N]^-$ anion, and carbon dioxide shown as a function of the number of carbon dioxide molecules per anion−cation pair (c) in the mixture of $[bmim]^+[Tf2N]^-$ with CO_2 at 298 K. The data were obtained by ^{13}C PFG NMR (a) and by MD simulation (b).

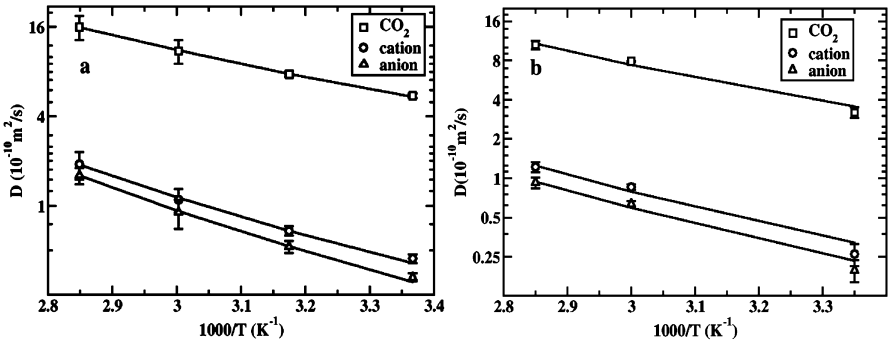

Figure 7. Examples of the temperature dependencies of the self-diffusivity in the mixture of $[bmim]^+[Tf2N]^-$ with CO_2 obtained by ^{13}C PFG NMR measurements (a) and MD simulations (b). The number of carbon dioxide molecules per anion−cation pair is 0.44. The lines show the best fit results using eq 5.

Table 2. Activation Energy of Diffusion (E_a (kJ/mol)) in $[bmim]^+[Tf2N]^-$−CO_2 Mixtures for Different Numbers of Carbon Dioxide Molecules Per Anion−Cation Pair (c)

	simulation			experiment			% difference		
c	CO_2	cation	anion	CO_2	cation	anion	CO_2	cation	anion
0	–	28_2	29_1	–	29_2	31_2	–	3.4	6.5
0.04	24_3	31_1	31_1	18_2	27_1	28_2	33.3	14.8	10.7
0.08	23_1	27.8_2	28.0_4	19_2	28_1	27_3	21.1	0.71	3.7
0.19	21.5_1	27_1	26_1	18_4	25_4	26_3	19.4	8	0
0.44	20_2	24_3	25_3	17_3	23_4	25_3	17.6	4.3	0

experiment is excellent. It was observed in both the simulations and experiments that the activation energies of the ions decrease with an increase in the amount of CO_2. As the mole fraction of CO_2 increases, a greater number of CO_2 molecules cluster around the anion, thereby reducing the electrostatic interaction between the cation and anion. This reduces the energy barrier for diffusion.

MD Results of Structural Properties and Short-Time Dynamics. *Density and Molar Volume.* Densities obtained from the *NPT* MD simulations at 298 K and different CO_2 compositions are listed in Table 3. The density predictions at 298, 333, and 351 K are provided in Figure 8 where the pure IL densities are also compared with experimental results.[34] The calculated densities of the pure IL at all temperatures agree within 1.5% of the experimentally measured densities.

It can be observed that the density of the mixture decreases with the increasing mole fraction of CO_2 in the system. Moreover, it can be inferred from Figure 8 that the decrease in density with the increase in CO_2 concentration is linear and almost identical for all the temperatures.

Table 3. Densities of $[bmim]^+[Tf2N]^-$−CO_2 Mixtures for Different Numbers of Carbon Dioxide Molecules Per Anion−Cation Pair (c) at 298 K

c	ρ (g/cm^3)
0	1.4617_{14}
0.04	1.4602_6
0.08	1.4586_6
0.19	1.4539_5
0.44	1.4448_3

To quantify the effect of CO_2 on the packing of IL, excess molar volumes V^E were calculated at different CO_2 compositions at 298 K

$$V^E = \frac{x_{IL}M_{IL} + x_{CO_2}M_{CO_2}}{\rho_{mix}} - x_{IL}V_{mIL} - x_{CO_2}V_{mCO_2} \quad (6)$$

where x, M, and V_m represent mole fraction, molecular weight, and molar volume of pure components, respectively, and ρ_{mix} is

dx.doi.org/10.1021/jp304528d | J. Phys. Chem. B 2012, 116, 9141−9151

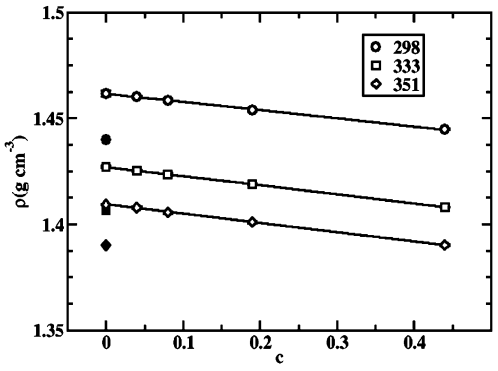

Figure 8. Densities of $[bmim]^+[Tf2N]^-$–CO_2 mixtures at different temperatures as a function of the number of carbon dioxide molecules per anion–cation pair (c). Simulation values are represented by open symbols and experimental[34] values are represented by closed symbols. The lines are linear fits to the data.

the density of IL–CO_2 mixture. The molar volume of CO_2 was calculated by assuming it to be an ideal gas, while the molar volume of IL was obtained from the simulation of the CO_2-free IL. The densities of IL-rich mixtures are not significantly affected even when applying very high pressures as was observed by Huang et al.[35] Therefore, instead of running a separate set of simulations at 1 bar for different CO_2 compositions, mixture densities for different pressures were used for the calculation of excess molar volume. Computed excess molar volumes for different CO_2 compositions at 1 bar are listed in Table 4.

Table 4. Excess Molar Volume (V^E (cm^3/mol)) in $[bmim]^+[Tf2N]^-$–CO_2 Mixtures for Different Numbers of Carbon Dioxide Molecules Per Anion–Cation Pair (c) at 298 K

c	V^a	V^E
0.04	277.2_1	-927.1_3
0.08	267.3_1	-1890.6_3
0.19	247.6_4	-3929.8_2
0.44	210.7_1	-7453.6_1

[a] V is mixture molar volume.

The excess molar volume of the solution is negative, which is consistent with the experimental[36,37] and simulation[37,38] results obtained for a large number of IL mixtures. The very large negative excess volume in the present case is attributed solely to the large molar volume of CO_2, which is 24 436 cm^3/mol as opposed to that of the IL which is 287 ± 1 cm^3/mol at standard temperature and pressure. Experimental molar volume of the same IL has been measured to be 293 ± 2 cm^3/mol by Aki et al.[39] From Table 4 it is also observed that the molar volume of the mixture decreases linearly with an increase in CO_2 concentration, about 24% for c = 0.44. The same behavior has been observed for a wide range of ILs.[39] However, there is no substantial increase in the total volume of the mixture with increasing concentration of CO_2. This is due to the very low partial molar volume of CO_2 which was calculated to be 39 ± 1 cm^3/mol. As Berne and co-workers have discussed,[35] such a low partial molar volume of CO_2 in IL is attributed to the spontaneous forming of cavities due to the angular arrangement of anions for the accommodation of CO_2.

Velocity Autocorrelation Function. The velocity autocorrelation function ($\Phi(t)$) provides a measure of how the velocity of a particle, at any time t, is correlated with respect to its velocity at time t = 0

$$\Phi(t) = \langle v(t)\cdot v(0)\rangle \tag{7}$$

where $v(t)$ is the velocity at time t and $v(0)$ is the velocity at time t = 0. The normalized $\hat{\Phi}(t)$ obtained from the simulations, defined as

$$\hat{\Phi}(t) = \frac{\langle v(t)v(0)\rangle}{\langle v(0)v(0)\rangle} \tag{8}$$

is plotted in Figure 9 for cation, anion, and CO_2.

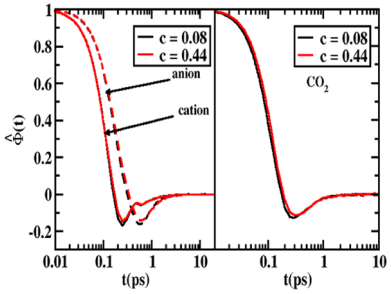

Figure 9. Normalized center of mass $\hat{\Phi}(t)$ at different composition of CO_2 in $[bmim]^+[Tf2N]^-$–CO_2 mixtures at 333 K.

From Figure 9, the total decorrelation time for all the species is observed to be about 3 ps. Molecular simulations[40,41] of different $[bmim]^+$-based ILs have shown that the decorrelation time in the range of 3 ps is typical of $[bmim]^+$ cations. The decorrelation in the velocity is observed due to the collision of a given molecule with neighboring molecules in the first solvation shell. This so-called initial rattling region appears as a negative correlation with the initial velocity. For CO_2 and the cation, the rattling region is observed at ~0.15 ps while for anion this region is about ~0.3 ps. Beyond the decorrelation time, the species diffuse out of the initial cage of molecules. Note that the self-diffusion coefficient computed via the Einstein relation was obtained on the time scale of 0.6–1 ns, well beyond the decorrelation times of all species. It is evident from Figure 9 that, with the increase in CO_2 concentration, the depth of the negative region of $\hat{\Phi}(t)$ becomes slightly less and can be ascribed to the presence of CO_2, which makes the cage wall softer.

Figure 10 shows the running integral of $\hat{\Phi}(t)$ which is related to the self-diffusion coefficient through the following Green–Kubo relationship

$$D = \int_{\infty}^{0} \frac{1}{3N} \sum_{i=1}^{N} \langle v(t)\cdot v(0)\rangle \, dt \tag{9}$$

The magnitudes of the running integrals are consistent with the self-diffusivities computed from the Einstein equation; CO_2 has the highest diffusivity followed by the cation and anion.

Dynamic Heterogeneity. The MSD quantifies how far a particle has displaced in a given time, while the self-part of the van Hove correlation function gives an idea about the distribution of the motion of a species. The self-part of the van Hove function[42] is given by

dx.doi.org/10.1021/jp304528d | J. Phys. Chem. B 2012, 116, 9141–9151

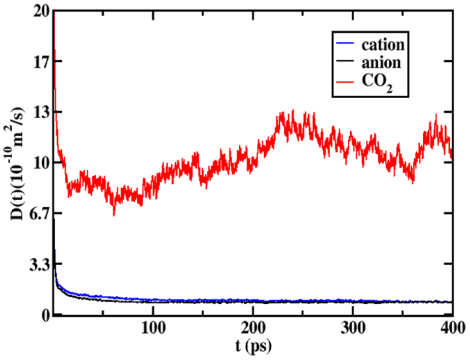

Figure 10. Running integrals of $\Phi(t)$ in $[bmim]^+[Tf2N]^-$–CO_2 mixtures at 333 K and c = 0.44.

$$G_s(r, t) = \frac{1}{N}\langle \sum_{j=1}^{N} \delta(r + r_j(0) - r_j(t))\rangle \quad (10)$$

where $G_s(r,t)$ is the probability that at a time t an atom has diffused a distance r from its original position corresponding to time t = 0. For typical liquids $G_s(r,t)$ has a Gaussian form given by[24]

$$G_s^d(r, t) = [3/2\pi\langle r^2(t)\rangle]^{3/2} \exp[-3r^2/2\langle r^2(t)\rangle] \quad (11)$$

The van Hove functions obtained from the MD simulations for CO_2, cation, and anion at a ratio of carbon dioxide molecules per anion–cation pair (c) of 0.44 are shown in Figure 11. The van Hove function for all the species is nearly

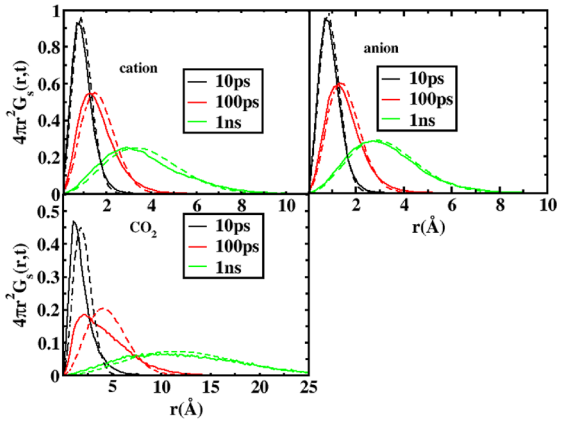

Figure 11. Self-part of van Hove correlation function in $[bmim]^+[Tf2N]^-$–CO_2 mixtures at 298 K and c = 0.44. Dashed line is a Gaussian fit.

Gaussian at 10 ps and 1 ns. However, at an intermediate time (100 ps), the van Hove function deviates significantly from the Gaussian distribution, suggesting that at these intermediate times there exists heterogeneity in the diffusion of each species. In the time regions of maximum non-Gaussian behavior it is observed that $G_s(r,t)$ and $G_s^d(r,t)$ intersect at around 3 Å for the cation and anion and around 6 Å for CO_2. This makes it evident that, although the majority of the ions are diffusing slowly compared to the Gaussian, there is a small number of highly mobile ions, characterized by long time tail of $G_s(r,t)$. In this regime, there are some species that are temporarily trapped by the counterion species. Only at long times can they escape this cage and enter the diffusive regime.[24] The long time tails of CO_2 are consistent with the fact that CO_2 has higher self-diffusion coefficients than the cation and anion. Also, it is noted that the cation has longer time tail than the anion, consistent with its higher self-diffusion coefficient. These results corroborate the results obtained from the MSD.

Rotational Correlation Function (C(t)). Rotational dynamics of all the species is quantified by computing the time correlation function $C(t)$, which describes how the rotational motion of a species is correlated at different times. It also provides a qualitative measure of the viscosity of the system, since slow rotational motion is correlated with high viscosity. The rotational correlation function is defined as

$$C(t) = \left\langle \frac{1}{2}[3\cos^2\theta_i(t) - 1] \right\rangle \quad (12)$$

where $\theta_i(t)$ is the angle between a vector at time t and time t = 0. The rotational time correlation function is usually fit to a stretched exponential function

$$C(t) = a_0 e^{-(t/\tau_0)^\beta} \quad (13)$$

where a_0 and τ_0 are constants and β is a stretching parameter. For the cation, the correlation function was computed along the vector connecting two terminal carbons, which is also the longest axis (see Figure 12), and along the plane normal to the

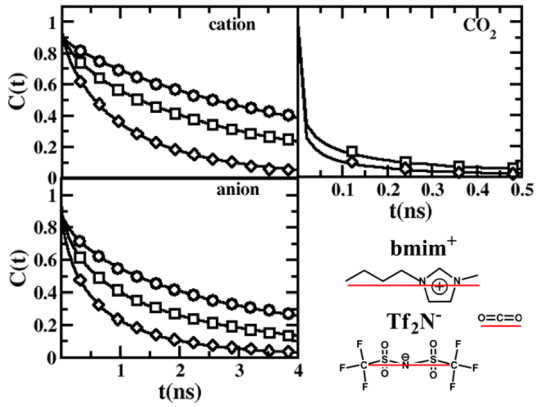

Figure 12. Rotational correlation function of cation, anion, and CO_2 in $[bmim]^+[Tf2N]^-$–CO_2 mixtures at 298 K and c = 0 (○), c = 0.19 (□), and c = 0.44 (◇). Solid line is the fit represented by eq 13.

ring given by the cross product of two vectors connecting a nitrogen atom associated with the butyl chain and two carbon atoms on the ring adjacent to it. For the anion, $C(t)$ was computed for the axis connecting two terminal carbons (see Figure 12) and a plane normal to the nitrogen atom which is given by the cross product of two vectors connecting a nitrogen atom and two sulfur atoms adjacent to it. Rotational motion of the vector connecting two oxygen atoms was studied for CO_2.

The rotational time correlation functions for all the species at two different CO_2 contents are shown in Figure 12. It is observed that the rotational correlation function of CO_2 decays faster followed by that of the anion and cation. This is because CO_2 is the smallest molecule and the cation is the largest. Interestingly, the cation rotates more slowly than the anion because of its longer axis, but its translational motion is faster than that of the anion. Also the correlation functions decay rapidly with an increasing amount of CO_2 in the system, which is consistent with the observation that CO_2 fluidizes the system, weakening the electrostatic forces that would have otherwise hindered the motion of the species.

dx.doi.org/10.1021/jp304528d | J. Phys. Chem. B 2012, 116, 9141–9151

Rotational time constants (τ) for each species were computed by integrating eq 13

$$\tau = \int_0^\infty C(t)\, dt \tag{14}$$

The rotational time constant is a measure of the time taken by a given species to decorrelate from its initial orientation. Rotational time constants for different vectors of the cation, anion, and CO_2 as a function of temperature and CO_2 composition are listed in Table 5.

Table 5. Rotational Time Constant (τ (ns)) in $[bmim]^+[Tf2N]^-$–CO_2 Mixtures for Different Numbers of Carbon Dioxide Molecules Per Anion–Cation Pair (c) and at Different Temperatures

		CO_2	cation		anion	
T (K)	c	molecular axis	molecular axis	normal	molecular axis	normal
298	0	–	1.0_1	0.3_1	0.9_1	0.17_2
	0.04	0.06_2	1.0_1	0.36_1	0.8_1	0.17_1
	0.08	0.049_3	0.9_1	0.31_3	0.7_1	0.15_2
	0.19	0.039_3	0.68_4	0.25_2	0.6_1	0.12_1
	0.44	0.026_1	0.5_1	0.17_2	0.38_4	0.08_1
333	0	–	0.25_1	0.09_1	0.20_1	0.041_2
	0.04	0.014_2	0.230_1	0.081_2	0.185_3	0.039_1
	0.08	0.012_1	0.23_1	0.08_1	0.18_1	0.038_2
	0.19	0.011_1	0.20_1	0.068_3	0.154_8	0.033_2
	0.44	0.008_1	0.138_2	0.050_3	0.110_4	0.025_1
351	0	–	0.15_1	0.051_2	0.12_1	0.026_2
	0.04	0.008_1	0.14_1	0.047_2	0.109_4	0.024_1
	0.08	0.007_1	0.130_5	0.044_2	0.104_4	0.023_1
	0.19	0.007_1	0.12_1	0.041_4	0.09_1	0.021_2
	0.44	0.0052_3	0.09_1	0.032_2	0.08_1	0.017_1

It is readily apparent that the rotational time constant of CO_2 is an order of magnitude smaller than those of the cation and anion, indicating rapid rotational motion of CO_2 owing to its smallest size among all the species. For the cation and anion, the rotational time constant is close to at least 0.5 ns at 298 K and the highest CO_2 loading. It can also be observed that the rotational time constants for the cation and anion along the molecular axis are larger than those computed for the vector normal. Once again this indicates that the rotational motion is slower along the molecular axis as compared to that along the normal direction.

As observed with the self-diffusion coefficients of all the species, the rotational time constants decrease with increasing temperature as well as increasing CO_2 loading, indicating that the viscosity of the system decreases as CO_2 is added. A decrease in viscosity of $[bmim]^+[NTf_2]^-$ upon addition of CO_2 has been experimentally shown by Laurenczy and Dyson.[43] From Table 5, it appears that at the lowest concentrations of CO_2 the rotational motion does not change much; it is only when CO_2 concentrations become high that the rotational time constants decrease significantly. This suggests that there is some critical concentration of CO_2 required to sufficiently fluidize the liquid, below which the viscosity should not change much.

The van Hove correlation functions of each species as a function of CO_2 concentration at 298 K are given in Figure 13. The correlation function of each species shows longer tails with increasing concentrations of CO_2, which is characteristic of a

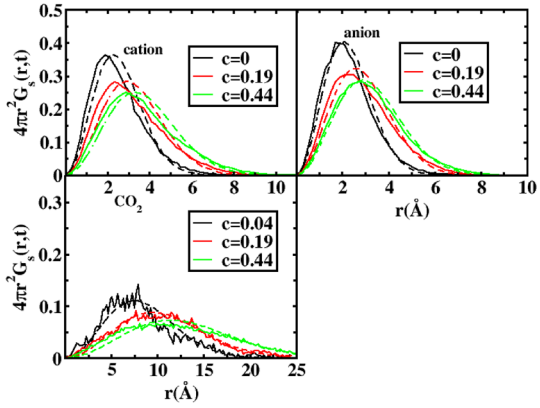

Figure 13. van Hove correlation function in $[bmim]^+[Tf2N]^-$–CO_2 mixtures at 298 K and 1 ns. Dashed line is a Gaussian fit.

higher diffusivity. Also, as the number of CO_2 molecules is increased, the motion of the ions becomes more Gaussian. This agrees with our initial hypothesis that CO_2 fluidizes the system, thereby making the diffusion more homogeneous.

Deviation from Gaussian behavior can be characterized by a non-Gaussian parameter given by

$$\alpha(t) = \frac{3\langle r^4(t)\rangle}{5\langle r^2(t)\rangle^2} - 1 \tag{15}$$

Gaussian dynamics are characterized by values of $\alpha(t) = 0$; the magnitude of the deviations of $\alpha(t)$ from zero gives an indication of the level of dynamic heterogeneity of the motion. From Figure 14 it is observed that, with increasing CO_2

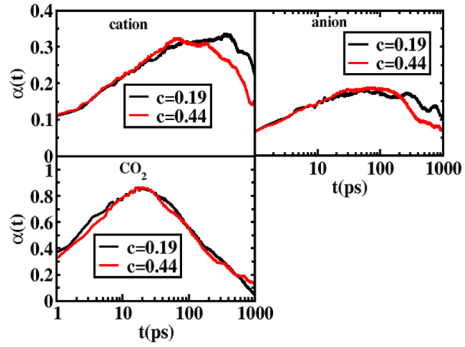

Figure 14. Non-Gaussian parameter in $[bmim]^+[Tf2N]^-$–CO_2 mixtures at 298 K for cations, anions, and CO_2 at two different CO_2 concentrations.

concentration, there is a decrease in the value of the non-Gaussian parameter $\alpha(t)$, corroborating the results obtained from the van Hove function. Also, it is observed that maximum value for $\alpha(t)$ shifts to longer times as the concentration of CO_2 decreases and the species takes longer time to reach the diffusive regime. The value of $\alpha(t)$ for the cation reaches a maximum at around 100 ps, while for anion the distribution is flatter with no obvious maximum. This confirms the result from the van Hove analysis that cations and anions show more deviation from the Gaussian behavior at a time scale on the order of 100 ps. However, for CO_2 the value of $\alpha(t)$ reaches a maximum at 20 ps and then goes to zero at about 1 ns, indicating that pure diffusive behavior is observed for CO_2 on the nanosecond time scale. For the cation and anion, however, it is observed that $\alpha(t)$ is still nonzero after 1 ns, suggesting

dx.doi.org/10.1021/jp304528d | J. Phys. Chem. B 2012, 116, 9141–9151

subdiffusive motion on this time scale. This is why for 298 K, and all composition of CO_2 studied here, trajectories longer than 1 ns are necessary to obtain reliable self-diffusion coefficients for the cation and anion.

The picture that emerges from the analysis above is as follows. CO_2 diffuses rapidly through a series of relatively long displacements, consistent with the van Hove analysis in Figure 11. This can also be observed in an animation of the fluid (see Supporting Information). The cations and anions, on the other hand, have much shorter displacements over the same period of time, again consistent with Figure 11. The latter behavior is due to the fact that the cations and anions associate strongly with one another via Coulombic interactions, so that motion is much more correlated. For this reason the diffusivities are nearly identical for the ions, in both the experiments (Figure 6a) and simulations (Figure 6b). Because CO_2 is neutral, it interacts mainly through weak van der Waals forces. Its motion is therefore weakly coupled with the motion of ions.

CONCLUSION

High-field and high-gradient PFG NMR technique was applied in combination with MD simulations to study self-diffusion in mixtures of CO_2 and the ionic liquid $[bmim]^+[Tf2N]^-$. In addition, MD simulations were used to investigate short-time dynamic properties and structural properties to gain a deeper insight into the dynamic behavior of these mixtures. It was observed that, although the self-diffusivities obtained by MD simulations are about 50% lower than the corresponding experimental values, there is a good agreement between the simulation and experimental data on the self-diffusivity ratios of the ions and CO_2 as well as on the dependencies of the self-diffusivities on the CO_2 content and temperature. For the studied temperature range, the temperature dependencies of diffusivities of all species in mixtures of CO_2 and $[bmim]^+[Tf2N]^-$ were found to be in agreement with the Arrhenius law. The activation energies of diffusion were found to be larger for the ions than that for CO_2. The diffusivity of the cation was found to be larger than that of the anion. In agreement with previous studies, this observation was explained by the preferential mobility of the cations in the direction of the ring plane. Addition of CO_2 into the ionic liquid was found to increase the ion self-diffusivities. This was attributed to fluidization of the system by CO_2 resulting in a decrease of the mixture density. The simulations predict that the excess molar volume of CO_2−$[bmim]^+[Tf2N]^-$ mixtures is large and negative, and the corresponding partial molar volume of CO_2 is about 39 cm^3/mol. This is due to the fact that CO_2 occupies cavities within the ionic liquid, which results in a small change in total volume, even for mole ratios of CO_2 as high as 0.44. A van Hove analysis as well as the velocity and rotational correlation functions show that CO_2 fluidizes the ionic liquid. Dynamic heterogeneities reach a maximum on a ∼100 ps time scale for the ionic liquid ions and a ∼20 ps time scale for CO_2. At 298 K CO_2 exhibits pure diffusion characteristics after about 1 ns, but subdiffusive behavior for the ions persists beyond 1 ns.

ASSOCIATED CONTENT

Supporting Information

Movie of an MD trajectory which shows CO_2 diffusion in the IL is provided. This material is available free of charge via the Internet at http://pubs.acs.org.

AUTHOR INFORMATION

Corresponding Author

*Phone: +1 574 631 5687 (E.J.M.); +1 352 392 0315 (S.V.). Fax: +1 574 631 8366 (E.J.M.); +1 352 392 0315 (S.V.). E-mail: ed@nd.edu (E.J.M.); svasenkov@che.ufl.edu (S.V.).

Notes

The authors declare no competing financial interest.

ACKNOWLEDGMENTS

We are grateful for the financial support of this work by the NSF CBET awards (No. 0967458 and 0967703). NMR data was obtained at the Advanced Magnetic Resonance Imaging and Spectroscopy (AMRIS) facility in the McKnight Brain Institute of the University of Florida. The NMR measurement time provided in the framework of the external user program of the National High Magnetic Field laboratory, AMRIS, is gratefully acknowledged. Members of the Vasenkov Group especially thank Dan Plant and Jim Rocca at AMRIS for help with NMR measurements. Computational resources were provided by Notre Dame's Center for Research Computing.

REFERENCES

(1) Welton, T. *Chem. Rev.* **1999**, *99*, 2071.
(2) Barrosse-Antle, L. E.; Bond, A. M.; Compton, R. G.; O'Mahony, A. M.; Rogers, E. I.; Silvester, D. S. *Chem. Asian J.* **2010**, *5*, 202.
(3) Taylor, A. W.; Licence, P.; Abbott, A. P. *Phys. Chem. Chem. Phys.* **2011**, *13*, 10147.
(4) França, J. o. M. P.; Nieto de Castro, C. A.; Lopes, M. M.; Nunes, V. M. B. *J. Chem. Eng. Data* **2009**, *54*, 2569.
(5) Castner, E. W.; Margulis, C. J.; Maroncelli, M.; Wishart, J. F. *Annu. Rev. Phys. Chem.* **2011**, *62*, 85.
(6) Ananikov, V. P. *Chem. Rev.* **2010**, *111*, 418.
(7) Tao, J.; Buxing, H. *Curr. Org. Chem.* **2009**, *13*, 1278.
(8) Bara, J. E.; Carlisle, T. K.; Gabriel, C. J.; Camper, D.; Finotello, A.; Gin, D. L.; Noble, R. D. *Ind. Eng. Chem. Res.* **2009**, *48*, 2739.
(9) Yoon, I.-N.; Yoo, S.; Park, S.-J.; Won, J. *Chem. Eng. J.* **2011**, *172*, 237.
(10) Anthony, J. L.; Anderson, J. L.; Maginn, E. J.; Brennecke, J. F. *J. Phys. Chem. B* **2005**, *109*, 6366.
(11) Lee, B.-C.; Outcalt, S. L. *J. Chem. Eng. Data* **2006**, *51*, 892.
(12) Cadena, C.; Zhao, Q.; Snurr, R. Q.; Maginn, E. J. *J. Phys. Chem. B* **2006**, *110*, 2821.
(13) Tokuda, H.; Hayamizu, K.; Ishii, K.; Susan, M. A. B. H.; Watanabe, M. J. *Phys. Chem. B* **2004**, *108*, 16593.
(14) Menjoge, A. R.; Dixon, J.; Brennecke, J. F.; Maginn, E. J.; Vasenkov, S. *J. Phys. Chem. B* **2009**, *113*, 6353.
(15) Hou, Y.; Baltus, R. E. *Ind. Eng. Chem. Res.* **2007**, *46*, 8166.
(16) Kortenbruck, K.; Pohrer, B.; Schluecker, E.; Friedel, F.; Ivanovic-Burmazovic, I. *J. Chem. Thermodyn.* **2012**, *47*, 76.
(17) Callaghan, P. T. *Principles of NMR Microscopy*; Clarendon Press: Oxford, UK, 1991.
(18) Kärger, J.; Ruthven, D. M. *Diffusion in Zeolites and Other Microporous Solids*; Wiley & Sons: New York, 1992.
(19) Cotts, R. M.; Hoch, M. J. R.; Sun, T.; Markert, J. T. *J. Magn. Reson.* **1989**, *83*, 252.
(20) Leach, A. R. *Molecular Modeling Principles and Applications*; Addison Wesley Longman Limited: Essex, England, 1998.
(21) Wang, J.; Wang, W.; Kollman, P. A.; Case, D. A. *J. Mol. Graphics Modell.* **2006**, *25*, 247.
(22) Frisch, M. J. *Gaussian 09, Revision A.1*; Gaussian Inc.: Wallingford, CT, 2009.
(23) Bayly, C. I.; Cieplak, P.; Cornell, W.; Kollman, P. A. *J. Phys. Chem.* **1993**, *97*, 10269.
(24) Liu, H.; Maginn, E. *J. Chem. Phys.* **2011**, *135*, 124507.
(25) Potoff, J. J.; Siepmann, J. I. *AIChE J.* **2001**, *47*, 1676.
(26) Shi, W.; Maginn, E. J. *J.Phys. Chem. B* **2008**, *112*, 2045.

(27) Plimpton, S. *J. Comput. Phys.* **1995**, *117*, 1. LAMMPS, http://lammps.sandia.gov/.
(28) Yan, T.; Burnham, C. J.; Del Pópolo, M. G.; Voth, G. A. *J. Phys. Chem. B* **2004**, *108*, 11877.
(29) Jiang, W.; Yan, T.; Wang, Y.; Voth, G. A. *J. Phys. Chem. B* **2008**, *112*, 3121.
(30) Bühl, M.; Chaumont, A.; Schurhammer, R.; Wipff, G. *J. Phys. Chem. B* **2005**, *109*, 18591.
(31) Chaban, V. V.; Voroshylova, I. V.; Kalugin, O. N. *Phys. Chem. Chem. Phys.* **2011**, *13*, 7910.
(32) Urahata, S. M.; Ribeiro, M. C. C. *J. Chem. Phys.* **2005**, *122*, 024511.
(33) Cadena, C.; Anthony, J. L.; Shah, J. K.; Morrow, T. I.; Brennecke, J. F.; Maginn, E. J. *J. Am. Chem. Soc.* **2004**, *126*, 5300.
(34) Tokuda, H.; Hayamizu, K.; Ishii, K.; Susan, M. A. B. H.; Watanabe, M. *J. Phys. Chem. B* **2005**, *109*, 6103.
(35) Huang, X.; Margulis, C. J.; Li, Y.; Berne, B. J. *J. Am. Chem. Soc.* **2005**, *127*, 17842.
(36) Lehmann, J.; Rausch, M. H.; Leipertz, A.; Fröba, A. P. *J. Chem. Eng. Data* **2010**, *55*, 4068.
(37) Anantharaj, R.; Banerjee, T. *Int. J. Chem. Eng.* **2011**, 2011.
(38) Gutowski, K. E.; Maginn, E. J. *J. Am. Chem. Soc.* **2008**, *130*, 14690.
(39) Aki, S. N. V. K.; Mellein, B. R.; Saurer, E. M.; Brennecke, J. F. *J. Phys. Chem. B* **2004**, *108*, 20355.
(40) Ishida, T.; Nishikawa, K.; Shirota, H. *J. Phys. Chem. B* **2009**, *113*, 9840.
(41) Kowsari, M. H.; Alavi, S.; Ashrafizaadeh, M.; Najafi, B. *J. Chem. Phys.* **2010**, *132*, 044507.
(42) Haile, J. M. *Molecular Dynamics Simulation Elementary Methods*; Wiley & Sons: New York, 1997.
(43) Laurenczy, G.; Dyson, P. J. *Z. Naturforsch. B Chem. Sci.* **2008**, 681.